Experimental Study of Codeposition Electrochemistry Using Mixtures of $ScCl_3$ and YCl_3 in LiCl-KCl Eutectic Salt at 500°C

Fuel Cycle Technology

Prepared for
U.S. Department of Energy
Materials Recovery and Wasteform Development Program
Michael R. Shaltry, Tae-Sic Yoo, and Guy L. Fredrickson
Idaho National Laboratory
August 31, 2017
NTRD-MRWFD-2017-000205

SUMMARY

This report fulfills the Level 3 Milestone No. M3FT-17IN030106022 titled "Experimental Study of Codeposition Electrochemistry Using $ScCl_3$ and YCl_3 in LiCl-KCl Eutectic Salt at 500 °C" within the Department of Energy (DOE) Work Package No. FT-17IN03010602 titled "Technology Gap-Study – INL." This work package falls under the Fuel Cycle Research and Development (FCR&D) Materials Recovery and Waste Form Development (MRWFD) Program 1.02.03.11 titled "Domestic Echem."

Cyclic voltammetry and chronopotentiometry tests were applied to molten LiCl-KCl eutectic at 500 °C including amounts of $ScCl_3$ and YCl_3. The purpose of the testing was to observe the effect of applied electrical current on the codeposition of scandium and yttrium, which were chosen as surrogate elements for uranium and plutonium, respectively. Features of the work were to vary the concentration of $ScCl_3$ (at relatively low concentrations) as well as varying the applied current, all with a fixed concentration of YCl_3. Results of the experiments could provide insight of uranium electrorefining and may provide evidence, which suggests the electrorefiner could be operated at lower UCl_3 concentration whereby codeposition (U and Pu) could be more effectively controlled.

CONTENTS

FIGURES

TABLES

ACRONYMS

Ag	Silver
AgCl	Silver Chloride
ANL	Argonne National Laboratory
CE	Counter Electrode
Cl	Chlorine
ClLiK	LiCl-KCl Eutectic
CP	Chronopotentiometry
CV	Cyclic Voltammetry
DOE	Department of Energy
ER	Electrorefiner
GC	Glassy Carbon
$GdCl_3$	Gadolinium Chloride
H_2O	Water
ICP-MS	Inductively Coupled Plasma- Mass Spectroscopy
INL	Idaho National Laboratory
LCC	Liquid Cadmium Cathode
Li	Lithium
MFC	Materials and Fuels Complex
$MgCl_2$	Magnesium Chloride
MRWFD	Material Recovery Waste Form Development
Ni	Nickel
NiO	Nickel Oxide
O_2	Oxygen
Pu	Plutonium
$PuCl_3$	Plutonium Chloride
RE	Reference Electrode
$ScCl_3$	Scandium Chloride
U	Uranium
UCl_3	Uranium Chloride
W	Tungsten
WE	Working Electrode
YCl_3	Yttrium Chloride
Zr	Zirconium

1. INTRODUCTION

1.1 Background

A result of recovering uranium from used nuclear fuel by the Pyroprocessing technology is Group 1, Group 2, lanthanide fission products metals, and transuranic metals accumulate in the electrorefiner (ER) salt. In order to retrieve the transuranic metals from the salt as a group, various chemical and electrochemical methods have been investigated. Electrochemical recovery of actinide metals is often referred to as 'codeposition.' Codeposition experiments related to Pyroprocessing have been ongoing at Idaho National Laboratory (INL) and Argonne National Laboratory (ANL) since approximately 2004.

The most widely studied codeposition process employs liquid cadmium as the cathode in which the transuranic metals are deposited as a group [Vaden]. A shortcoming of the liquid cadmium cathode (LCC) is a nontrivial level of lanthanide metals is included in the cathode deposit, which is not desirable when the intended use of the metals is to produce recycled nuclear fuel.

In addition to the LCC testing, some effort was devoted to testing a solid metal cathode. More recently, studies by ANL [Cruze, Tylka, Willit] and INL have placed emphasis on developing a solid cathode technology. An extensive list of reports related to codeposition work can be found in a previous report [Fredrickson].

Lab-scale experiments repeatedly indicate the deposition potentials of the major lanthanide species to the solid cathode are significantly lower than actinides. Taking advantage of the thermodynamic difference between the lanthanide and actinide reduction, a group actinide recovery process using a solid cathode has received attention from the Department of Energy (DOE) Material Recovery Waste Form Development (MRWFD) Campaign as an alternative to the LCC method. With the assumption of a well-designed electrochemical process that can regulate the cathodic deposition potential accurately, the cathode product should exhibit a lower impurity level of lanthanides.

Based on the most recent experiments with Mark-IV ER salt [Gese, Shaltry], realizing a process for handling a meaningful scale of the solid cathode proved to be challenging. The elevated amperage due to a rapidly increasing cathode surface and the required resistive voltage component interpretation poses a significant engineering difficulty to regulate the cathode potential, which is the most important parameter to control in order to deposit the actinides and leaving behind the lanthanides in a precise manner.

It is important to note solid cathode codeposition is routinely performed in the context of uranium-zirconium (U-Zr) recovery at the INL Materials and Fuels Complex (MFC) for the metal fuel processing campaign utilizing the Mark-IV ER. The operation oxidizes Zr dissolved in the cadmium pool in the Mark-IV ER and recovers U and Zr at the solid cathode together. Even though the operation only regulates the electrochemical cell current and the cathode potential is not carefully monitored, a typical result exhibits 10 to 20 wt % Zr in the cathode deposit with the balance being U metal. In this operation, the Zr concentration of the Mark-IV ER salt is initially zero and is expected to be at a level low enough to force the diffusion-limited behavior of Zr throughout electrochemical operation.

In the context of uranium-plutonium (U-Pu) codeposition process, the U-Zr recovery process seem to provide an obvious way to mitigate a prescribed difficulty in precisely controlling the cathode potential and the rapid increase of the cell current due to increased cathode surface area. However, a constraint is that, due to a safeguard concern, the operation may need to maintain a non-zero concentration of UCl_3 in the ER salt. Also, operating at a higher UCl_3 concentration for U recovery is likely to benefit process throughput and inefficiency.

1.2 Motivation

From the perspective of U recovery, the operation would be at a higher U concentration in the ER salt in order to preserve the purity of the uranium product and process throughput. However, from the perspective of U-Pu recovery, the operation would be better controlled with a lower U concentration. The concept of operating the ER at a relatively low UCl_3 concentration in the salt provides the motivation for this research.

1.3 Goal

The ultimate goal is to identify such key parameters as 1) the lowest possible UCl_3 concentration, which allows high purity U metal recovery and high process throughput and 2) the highest possible UCl_3 concentration, which can provide a U-Pu codeposit, containing a satisfactory amount of Pu, without incurring cell current overshoot. As the first step toward identifying these key parameters, we determine and investigate a suitable surrogate system, and define the methodology for identifying the two limiting concentrations.

1.4 Approach

1.4.1 UCl_3 and $PuCl_3$ Surrogates

Identifying the chemical potentials of the elements in the target system gives a gauge for the separation performance under an electrochemical operation. Thus, one can argue that the behavior of the U and Pu in the molten salt system can be emulated via surrogate elements exhibiting a similar chemical potential difference. Cyclic voltammetry (CV) is a useful tool for identifying chemical potential values.

To facilitate determining suitable U and Pu surrogates, the difference in reduction and oxidation potentials can be estimated from literature. Shirai et al. reported CV plots for U and Pu in LiCl-KCl at 500 °C [Shirai]. Based on graphical inspection of the reported CV data, the estimated potential difference between reduction and oxidation peaks for U and Pu is 294 mV. Thus, two surrogate chloride compounds with a similar potential difference are sought.

Unfortunately, in the search of literature for suitable surrogates it was found the published CV data varied by choice of reference electrode (RE), which makes comparison inconvenient. It is noted, that for measurements made with differing REs (at a common temperature) the potentials may be shifted, but the relationship among reduction potentials of elements is the same. The analyte chloride compounds chosen as candidates for this research were yttrium chloride (YCl_3), gadolinium chloride ($GdCl_3$), magnesium chloride ($MgCl_2$), and scandium chloride ($ScCl_3$).

In the following calculations, the potential differences are calculated based on the oxidation peaks. The oxidation peaks were used for this exercise because they were the most easily identified in plots taken from the published manuscripts. By subtracting the oxidation peak potential of a given species from the oxidation peak potential of lithium (Li), one can effectively set or the Li peak as the reference. This method eliminates the complication of comparing data measured against differing REs. For example,

$$\mathcal{E}_x = E_{Li} - E_x \quad (1)$$

where E is oxidation peak potential (volt) and the subscript Li and x refer to the species of lithium and another specified elemental species, respectively, and $\mathcal{E}_x$ is the potential difference between Li and the specified species. A negative value of $\mathcal{E}_x$ indicates the oxidation peak potential of the species x is positive in relation to that of Li.

Furthermore, calculating the difference between two specified elemental species should provide an estimate of the difference between the oxidation peaks of the two specified elements. For instance,

$$\mathcal{E}_{x,y} = \mathcal{E}_x - \mathcal{E}_y \quad (2)$$

Martinez et al. report measurements of $MgCl_2$ in LiCl-KCl eutectic (ClLiK) using a tungsten (W) working electrode (WE) and Mg RE. [Martinez] At (400, 550, and 727) °C, the difference between the Li and Mg oxidation peaks ($\mathcal{E}_{Mg}$) is approximately (0.64, 0.67, and 0.69) V. By interpolation and at 450 °C

$$\mathcal{E}_{Mg} \cong -0.65\ \text{V} \quad (3)$$

Castrillejo et al. report measurements of $ScCl_3$ in ClLiK using a W working electrode and a silver/silver chloride (Ag/AgCl) RE. [Castrillejo 2012] At 450 °C, the difference between the Li and Sc oxidation peaks is ~ 0.77 V.

$$\mathcal{E}_{Sc} \cong -0.77\ \text{V} \quad (4)$$

Bermejo et al. report measurements of $GdCl_3$ in ClLiK using a W working electrode and Ag/AgCl RE. [Bermejo] At 450 °C, the difference between the Li and Gd oxidation peaks is approximately 0.54 V.

$$\mathcal{E}_{Gd} \cong -0.54\ \text{V} \quad (5)$$

Castrillejo et al. report measurements of YCl_3 in ClLiK using a W working electrode and chlorine/chloride (Cl_2/Cl^-) RE. [Castrillejo 2003] At 450 °C,

$$\mathcal{E}_{Y} \cong -0.47\ \text{V} \quad (6)$$

A graphical representation of the CV plots of the data referenced above is shown in Figure 1 below. In this situation the curves are aligned to the Li oxidation peak. It can be seen the largest estimated difference between oxidation peaks is between Sc and Y whereas the smallest is between Gd and Y, as is indicated by the calculations listed in Table 1.

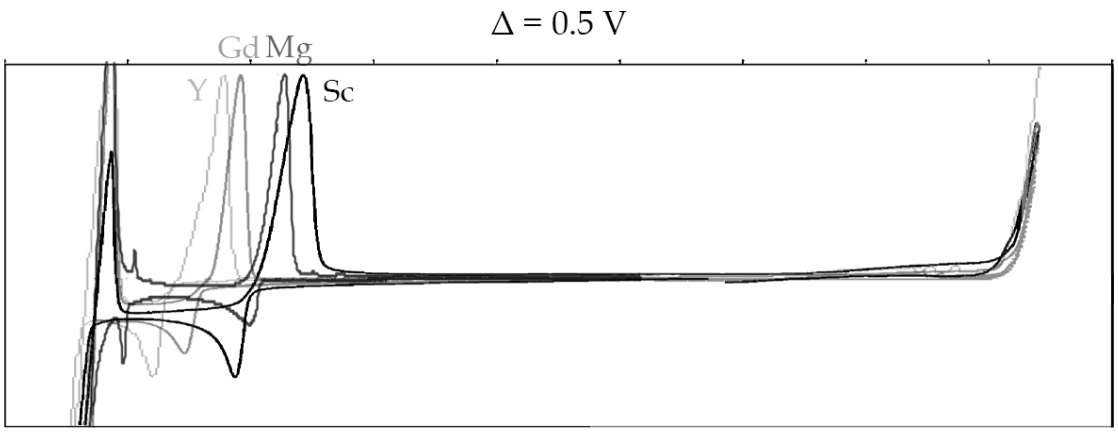

Figure 1: Overlay image showing the relationship among single element CV plots taken from literature as referenced in the text. Overlay generated courtesy of J. Seth Dustin (Center for Advanced Energy Studies-University of Idaho).

Table 1: Values indicating the potential difference (Ɛx,y) among oxidation peaks of elements, which were taken from literature.

Species		***Gd***	***Mg***	***Sc***
	$\mathcal{E}_x$ (V) / $\mathcal{E}_y$ (V)	**- 0.54**	**- 0.65**	**- 0.77**
Y	**- 0.47**	-0.07	-0.18	-0.3
Gd	**- 0.54**		-0.11	-0.23
Mg	**- 0.65**			-0.12

2. EXPERIMENTAL

2.1 Equipment and Materials

The electrochemical experiments were performed within an MBraun sealed atmosphere glovebox. The inert atmosphere was argon gas, which was conditioned to maintainwater and oxygen (H_2O and O_2) concentrations below 5 ppm. The chloride salts were heated by a 120 V Kerr Casting Electromelt furnace.

Electrochemical measurements were obtained by controlling a Princeton Applied Research VersaSTAT 4 potentiostat with VersaStudio potentiostat software.

Lithium chloride – potassium chloride eutectic (ClLiK) was used and the supporting electrolyte for the testing. The composition of ClLiK is 58.0 mol% LiCl and 42 mol% KCl (44.0 wt% and 56.0 wt%, respectively). Gadolinium chloride ($GdCl_3$), $MgCl_2$, YCl_3, and $ScCl_3$ were all anhydrous salts procured from Alfa Aesar.

The salt mixtures were contained by a glassy carbon crucible (HTW-Germany GAT 19) and maintained at 500 °C. Salt temperature was measured using a type-K thermocouple.

Measurements were obtained using a three-electrode configuration of which the working electrode (WE) and counter electrode (CE) were tungsten (Alfa Aesar) and the RE was nickel/nickel oxide, glassy carbon, or nickel metal. The nickel/nickel oxide (Ni/NiO) RE was prepared by placing NiO (Alfa Aesar) in a magnesium oxide (MgO) tube (Ozark Technical Ceramics), which was plugged with pourous MgO at one end. A nickel metal wire (Alfa Aesar) was then positioned within the MgO tube and in contact with the NiO.

2.2 Procedure

The surface area of the working electrode was controlled by placing the tungsten conductor within an alumina tube and sealing the bottom end with alumina paste. Multiple working electrodes were prepared this way. Differences in surface area were accounted for in measurements by calculating current density.

For each experiment, 50 g of ClLiK was used as the base electrolyte. After salts were placed in to the glassy carbon crucible, the crucible was placed into the furnace. Prior to switching on the furnace the electrodes were positioned in the furnace, but above the salt, to preheat. After approximately two hours the furnace had reached steady temperature and the salt had become fully molten. At that time the electrodes were lowered into the molten salt and acquisition of electrochemical data commenced.

3. RESULTS AND DISCUSSION

In certain electrochemical systems, such as those with electrolytes whose conductivity is low, resistance compensation may be necessary to ensure the electric potential imposed upon the working electrode is that which is desired. This resistance is referred to as 'uncompensated resistance' or '*IR* drop.' The potentiostat and software utilized for this work includes an *IR* drop determination function, which employs impedance spectroscopy. In performing the procedure for this electrochemical system, the result was the *IR* drop was negligible and no compensation was recommended. Therefore all electrochemical measurements were obtained without compensation.

Amongst the content, which follows, some data were analyzed and presented as the mean (μ), standard deviation (σ), and coefficient of variation ($c_v = \sigma\,\mu^{-1}$).

3.1 Reduction Potential Determination

The reduction potentials of Sc, Y, and Li were determined by finding the intersection of lines fitted to the regions around the onset. Onset of reduction is the location on the CV where current begins to change rapidly. Figure 2 shows the scheme graphically.

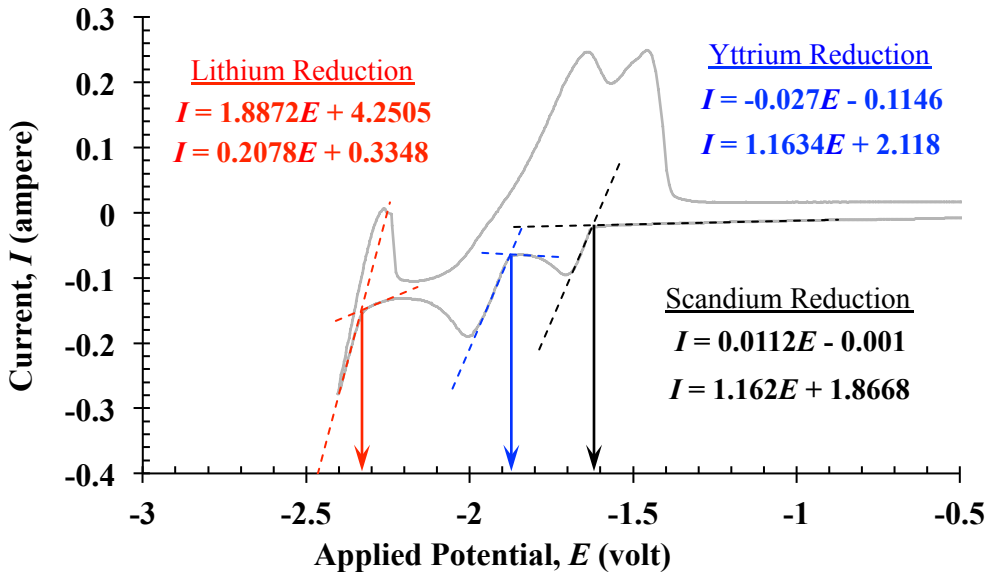

Figure 2: Graphic representation of the method utilized to determine the reduction potentials (onset) of scandium (black dashed lines), yttrium (blue dashed lines), and lithium (red dashed lines). The CV shown represents the (2.0 YCl_3 + 0.75 $ScCl_3$) wt% salt mixture.

3.2 Preliminary Mixtures and Measurements

Baseline CV measurements were made of ClLiK at 500 °C without any analyte compound present. The geometric surface areas of the WE used for the measurements made with the glassy carbon (GC), nickel (Ni) metal, and Ni/NiO REs were (0.864 & 0.707, 1.16, and 0.911) cm^2, respectively. The difference in WE surface area is accounted for by calculating current density, i (A cm^{-2}). Among all the measurements acquired, the common features of the curves are lithium redox couples, chlorine oxidation peak, and no significant peaks between the two aforementioned. Of the measurements made of ClLiK alone, the values of the mean and standard deviation for the electrochemical window are (3.70 ± 0.0077) V. The electrochemical window is the potential difference between the onset of lithium reduction (left side of CV plot) and the onset of chlorine oxidation (right side of CV plot). The CV plots of ClLiK are shown by Figure 3.

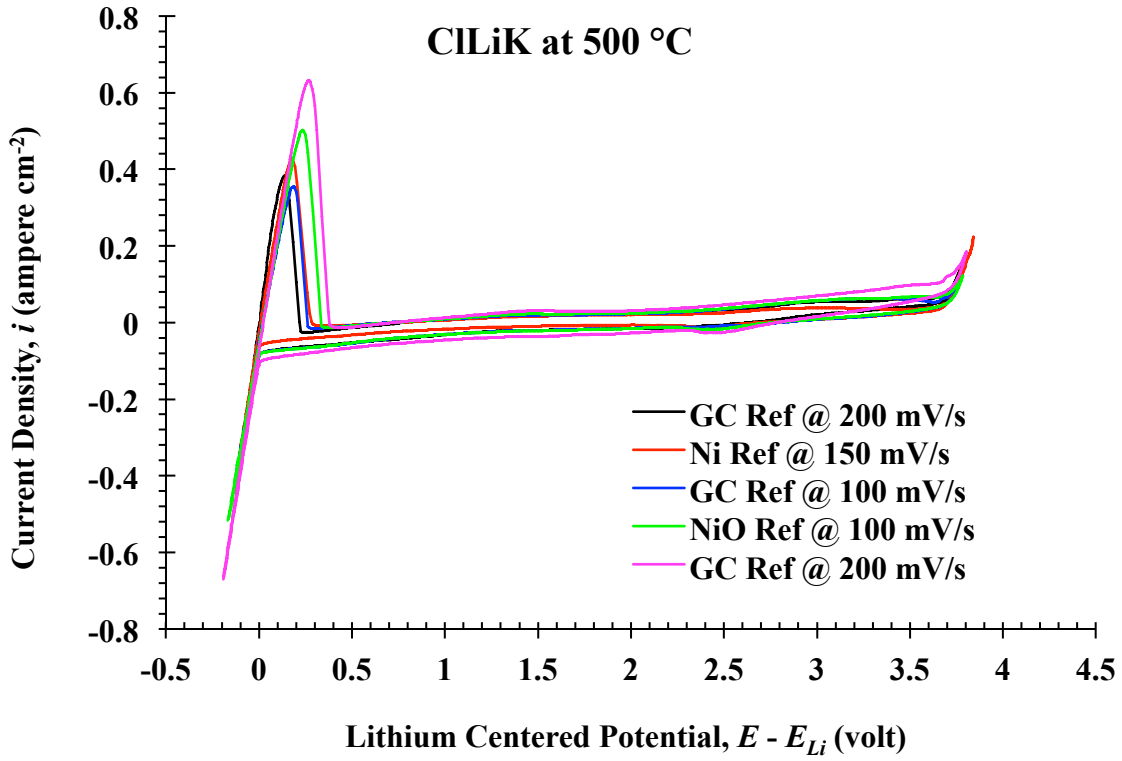

Figure 3: Cyclic voltammetry plots of tungsten in ClLiK at 500 °C. The plots shown were produced using different reference electrodes and scan rates as indicated.

It is important to highlight the fact that the curves shown in Figure 3 were obtained using different REs as well as scan rate. For ultimate consistency, a single RE should be used. However, by centering the CV data it is shown the curves can be compared. Centering the data is performed by subtracting the lithium reduction potential (E_{Li}) from all of the potential data points in the CV. Thus, the zero on the *x*-axis appears at lithium reduction. This method is referred to as 'lithium-centering.'

This is possible because the relationship of the thermodynamics among electrochemical reactions is independent of choice of RE. This is valid as long as the RE potential does not drift during measurement as well as all else remains constant, e.g. temperature.

Figures 4 and 5 display the CV plots obtained with an analyte compound added to the ClLiK salt. Each curve was generated of an individual chloride compound to the salt. The weight percent of $ScCl_3$, $GdCl_3$, YCl_3, and $MgCl_2$ in the salt was produced by adding (0.147, 0.25, 0.190, and 0.138) g, respectively. By adding a chloride compound the calculated electrochemical window is slightly smaller and is (3.64 ± 0.020) V. Figure 4 shows the analyte CV plots as lithium-centered potentials on the abscissa. Figure 5 shows the analyte CV plots as chlorine-centered potentials on the abscissa.

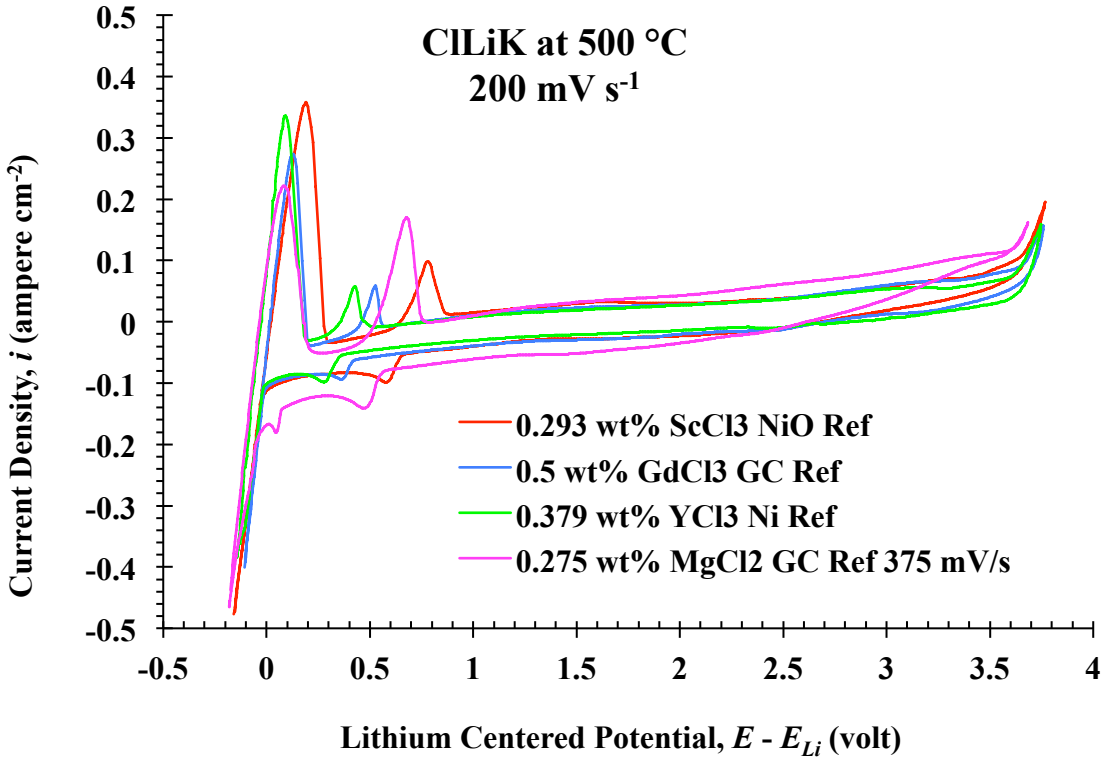

Figure 4: Cyclic voltammetry plots of various analytes in ClLiK at 500 °C. The measurements were made at a scan rate of 200 mV s^{-1} with the exception of the $MgCl_2$ curve being 375 mV s^{-1}. The curves were centered to the lithium reduction onset potential.

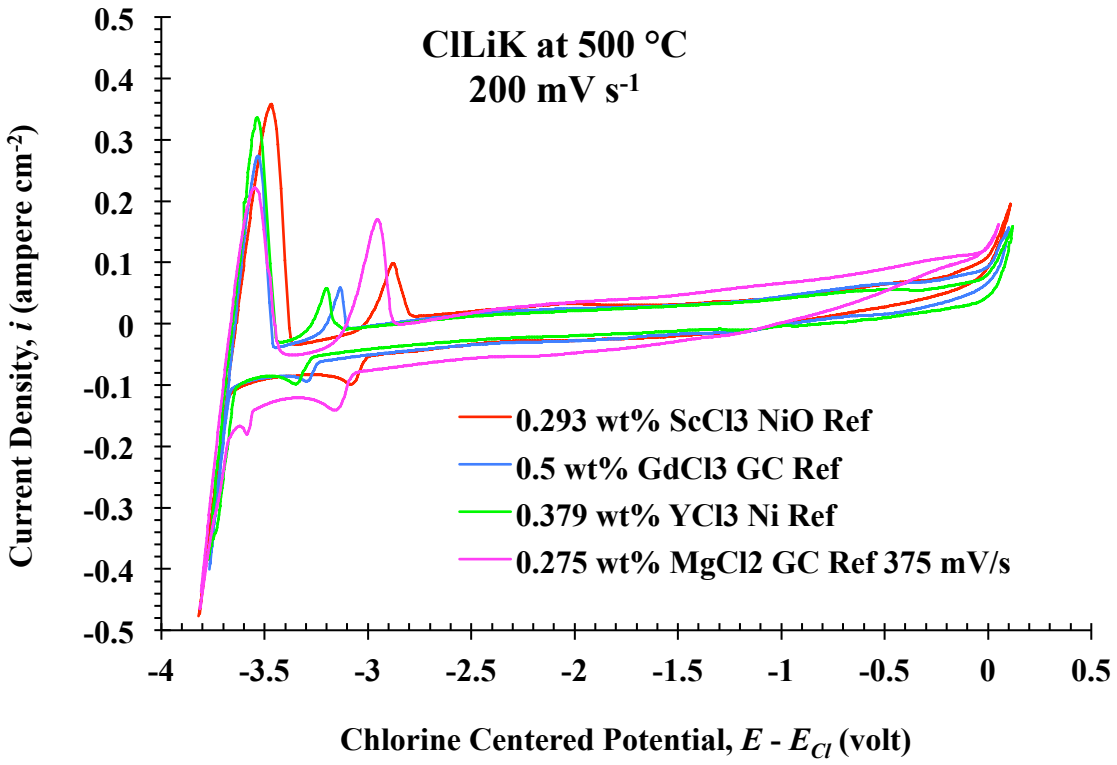

Figure 5: Cyclic voltammetry plots of various analytes in ClLiK at 500 °C. The measurements were made at a scan rate of 200 mV s^{-1} with the exception of the $MgCl_2$ curve, which was 375 mV s^{-1}. The curves were centered to the chlorine oxidation onset potential.

In comparing the lithium versus chlorine centering of CV data, it can be seen the relationship of the reduction and oxidation peaks are essentially the same, although there are differences to a small extent. From a practical standpoint either method of centering could be utilized, but there may be instances where one would be a better choice than the other. For the purpose of this research, lithium centering was chosen over chlorine as the onset of lithium reduction tends to be more distinct.

Comparing the plots shown in Figures 4 and 5 to the curves shown in Figure 1, it can been seen the relationship of the Li, Y, Gd, Mg, and Sc reduction and oxidation are reasonably consistent, which provides confidence in the method of centering the CV.

Table 2 lists the values determined of the lithium reduction and chlorine oxidation potentials as well as the calculated electrochemical window and the lithium-centered reduction potential of the given analyte species. The table also includes the overall average and standard deviation of the electrochemical window, which is (3.67 ± 0.033) V. The low value of c_v related to the electrochemical window calculation shows the thermodynamic relationship between lithium reduction and chlorine oxidation is consistent and independent of choice of RE. This in turn provides some confidence that the method by which the CV measurements of the salt mixtures in this work being compared is reasonable.

Table 3 lists the difference of reduction potentials among the analyte species based on the lithium-centered values listed in Table 2.

Table 2: List of lithium reduction and chlorine oxidation potentials as well as the calculated electrochemical window of ClLiK at 500 °C.

		Potential (volt)			
Analyte	***Reference***	***Li Reduction***	***Cl Oxidation***	***Window***	***Li-Centered Reduction***
-	GC	-1.318	2.386	3.704	-
-	Ni	-2.284	1.409	3.693	-
$GdCl_3$	GC	-1.836	1.824	3.660	-0.422
$GdCl_3$	GC	-1.546			-0.432
YCl_3	Ni	-2.282	1.346	3.628	-0.357
YCl_3	Ni	-2.288	1.346	3.634	-0.357
-	NiO	-2.157	1.545	3.702	-
-	GC	-0.988	2.704	3.691	-
$ScCl_3$	NiO	-2.072	1.588	3.660	-0.649
$ScCl_3$	GC	-1.037	2.632	3.669	-0.618
-	GC	-1.380	2.334	3.715	-
-	GC	-1.383	2.320	3.703	-
$MgCl_2$	GC	-1.506	2.126	3.631	-0.576
$MgCl_2$	GC	-1.509	2.099	3.608	-0.552
-	GC	-1.318	2.386	3.704	-
μ		-	-	3.67	-
σ		-	-	0.033	-
$\lvert c_v \rvert$		-	-	0.919	-

Table 3: Difference of reduction potentials (onset) in volts (lithium-centered) of single analyte mixtures.

	Gd	***Y***	***Sc***
Gd	-	-	-
Y	-0.070	-	-
Sc	0.207	0.277	-
Mg	0.137	0.207	-0.070

3.3 YCl_3-$ScCl_3$-ClLiK Mixtures

Based on the information presented in Sections 1.4.1 and 3.1, YCl_3 and $ScCl_3$ were chosen as $PuCl_3$ and UCl_3 surrogates, respectively. In 50 g of ClLiK, the concentration of YCl_3 was fixed at 2.0 wt % (1.02 g added) and the concentration of $ScCl_3$ was adjusted to (0.25, 0.5, 0.75, and 1.0) wt % (a total of 0.508 g added). The electrochemical measurements were obtained using tungsten as the WE and counter electrode (CE). The geometric surface area of the WE for all of the YCl_3-$ScCl_3$-ClLiK mixtures was 0.911 cm^2. Nickel metal was utilized as a RE. The bulk electrolyte was ClLiK eutectic at 500 °C.

3.3.1 Cyclic Voltammetry

Figure 6 displays the CV plots as measured and without the lithium peaks. Table 4 lists the reduction peak potentials for Sc and Y as well as their differences. The peak potentials of Sc and Y vary and the magnitude of current depends on the scan rate and the WE surface area. Typically, a higher scan rate and/or larger surface area produce a larger current peak. Surface area dependency of CV plots can be eliminated by converting current measurement to current density estimate. In theory, the scan rate dependency of CV plot can also be eliminated by scaling the peak current with square root of the scan rate. Though being sound in principle, subtle uncertainties are involved in scaling current measurements such as the surface area estimation and modeling assumption. Below, a method to mitigate the impact of uncertainties by taking advantage of the experiment specifics is provided.

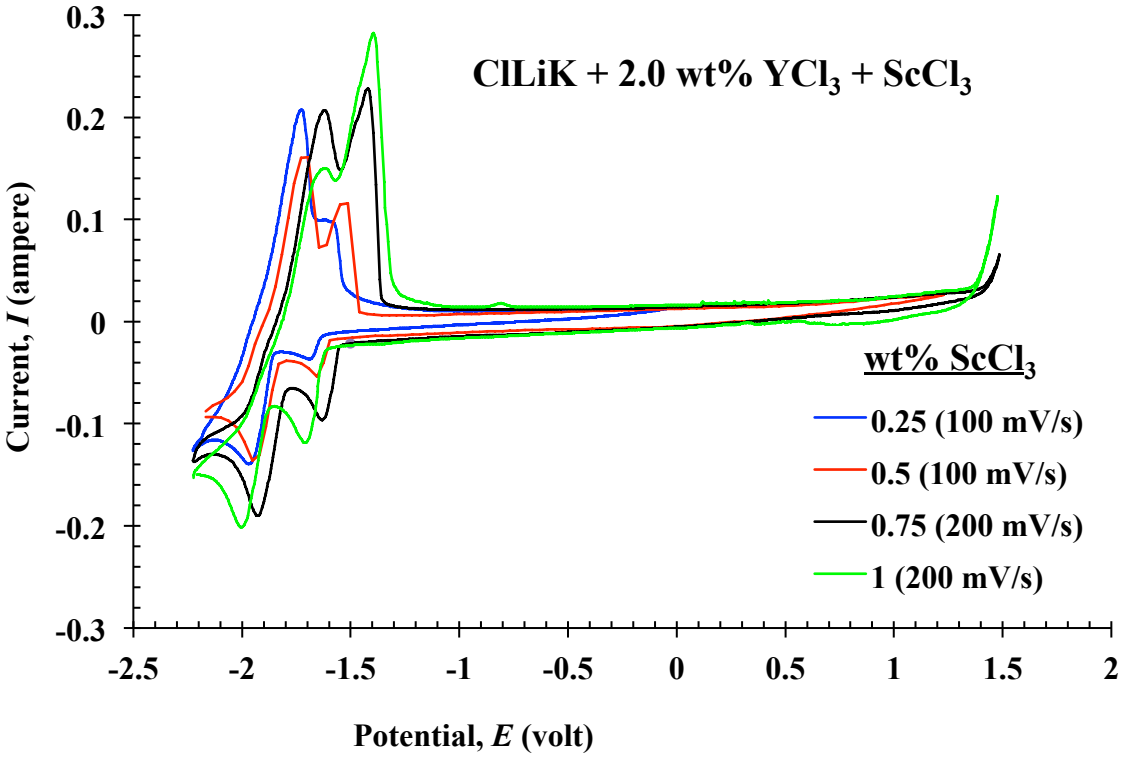

Figure 6: Raw cyclic voltammetry data measured versus nickel metal reference at 500 °C. The potential window was adjusted to not include lithium reduction and oxidation peaks.

Table 4: Scandium and yttrium reduction peak potentials and their potential difference.

wt% $ScCl_3$	***Reduction Peak Potential*** (volt)		***Potential Difference***
	Sc	***Y***	***Sc - Y***
0.25	-1.682	-1.965	0.283
0.5	-1.654	-1.950	0.296
0.75	-1.650	-1.932	0.282
1.0	-1.719	-2.008	0.289

Figure 7 displays manipulated CV plots, which allow for a more direct comparison. In this case the *x*-axis are potentials centered on the Y peak potential ($E_{Y,p}$) and dividing by the magnitude of the peak Y current ($I_{Y,p}$) the *y*-axis data are normalized and non-dimensionlized. It should be noted by normalizing by $I_{Y,p}$ the effect of scan rate is accounted for implicitly. Following data adjustment, the Sc reduction peaks align and increase in magnitude with concentration as expected.

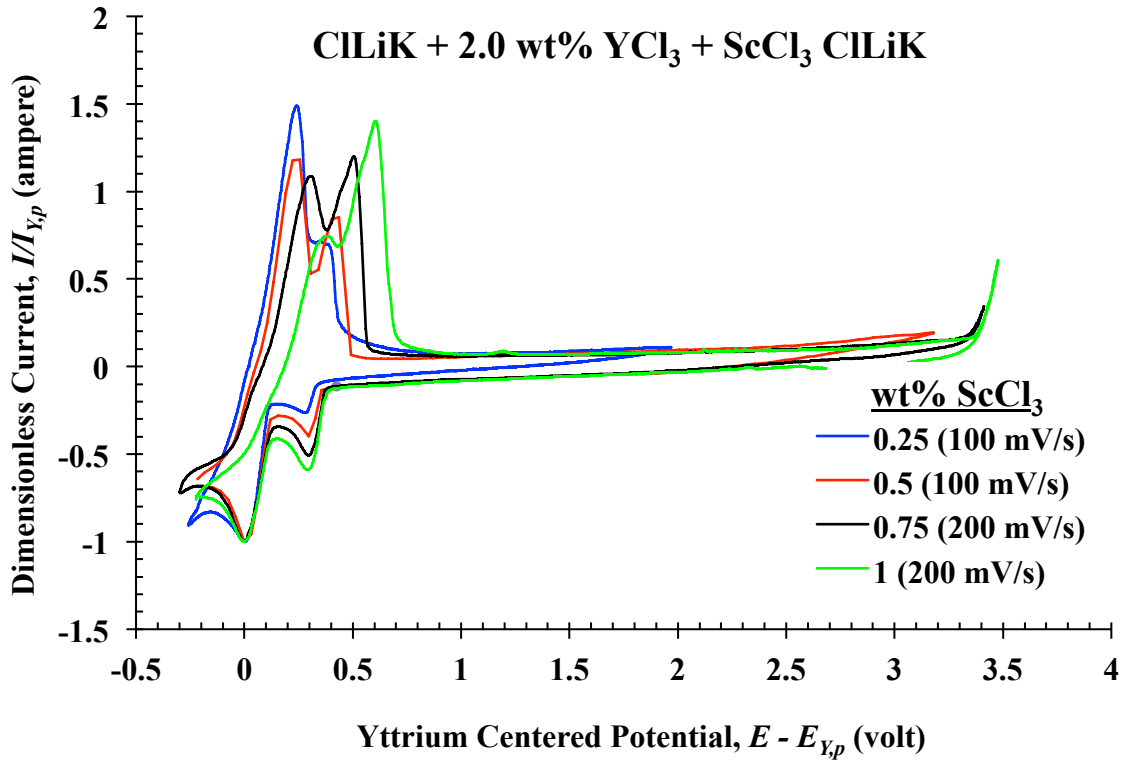

Figure 7: Adjusted cyclic voltammetry data measure versus nickel metal reference at 500 °C. The *x*-axis is centered with respect to the yttrium reduction peak potential ($E_{Y,p}$). The *y*-axis is normalized to the yttrium reduction peak current ($I_{Y,p}$).

Figure 8 displays manipulated CV plots, but in this instance the potentials are centered by the lithium reduction potential. Lithium centering produces alignment of the Y and Sc peak potentials. It should be noted the CV curves shown in Figure 8, which include reduction and oxidation peaks of Li, are not the same measurements as shown in Figure 7. Table 5 lists the onset reduction potentials for Sc, Y, and Li as well as their differences at each of the $ScCl_3$ concentrations.

In the situation where including the Li peaks in the CV is not desirable or achievable, centering the potential data to another peak in the CV could be useful, such as that which is shown by yttrium-centering of potential and Y current peak non-dimensionalizing. This method is best suited for an electrochemically active species in the molten salt whose concentration is not changing, which resembles an internal standard of sorts.

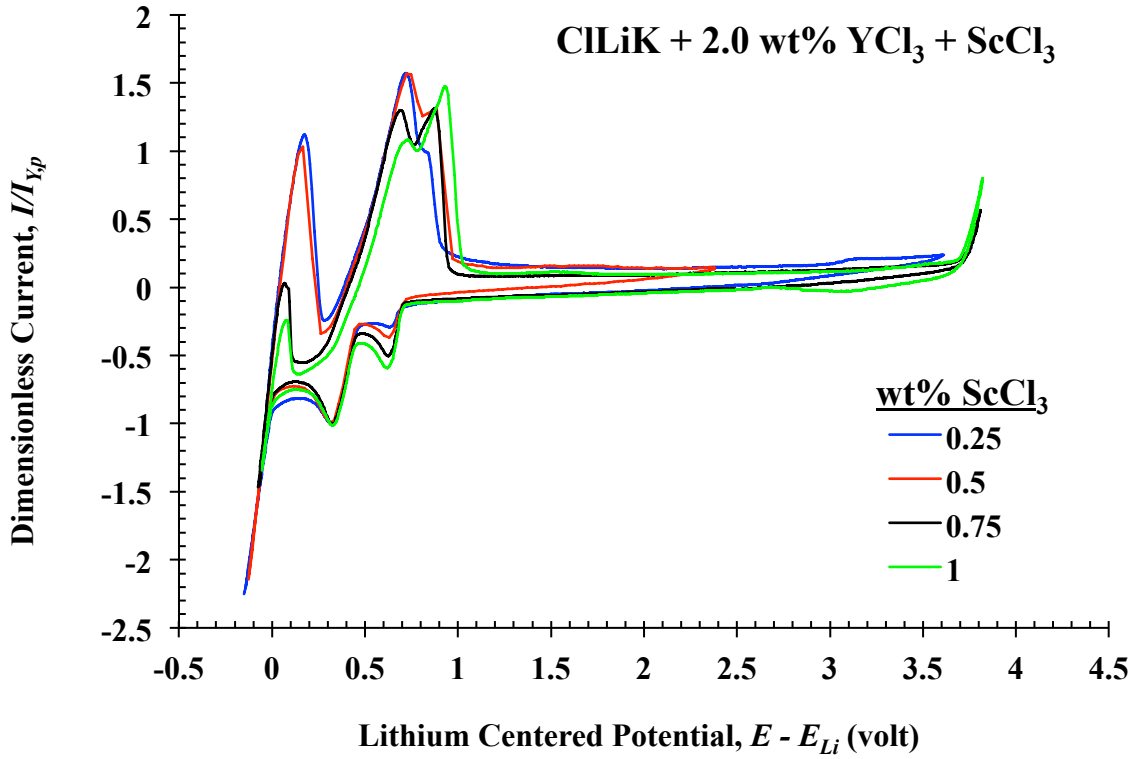

Figure 8: Adjusted CV data plotted with $ScCl_3$ concentration as a parameter. The *y*-axis values were non-dimensionalized and the *x*-axis values were centered about the lithium reduction potential. The potential window of the measurements was adjusted to include lithium reduction.

Table 5: List of reduction potentials (onset) and potential differences at each of the $ScCl_3$ concentrations.

wt% $ScCl_3$	***Reduction Onset Potential*** (volt)			***Potential Difference*** (volt)		
	Sc	***Y***	***Li***	***Sc - Li***	***Y - Li***	***Sc - Y***
0.25	-1.659	-1.910	-2.370	0.711	0.460	0.251
0.5	-1.683	-1.947	-2.399	0.716	0.453	0.263
0.75	-1.622	-1.875	-2.330	0.708	0.455	0.253
1.0	-1.646	-1.906	-2.351	0.705	0.445	0.260

3.3.2 Chronopotentiometry

It is noted here the potentials reported of the chronotpotentiometry (CP) data are those that were measured. There was no centering or shifting of the potential values in the presentation of or analysis of the CP data. The reduction potentials of Sc and Y were estimated based on features observed in the CP plots. In the plots, which follow, the average value for the Sc and Y reduction potentials are indicated by blue and black dashed lines, respectively.

Figures 9-12 display CP curves at various applied currents and Tables 6-9 list the estimated reduction potentials of Y and Sc for each of the four specified concentrations of $ScCl_3$ in the salt.

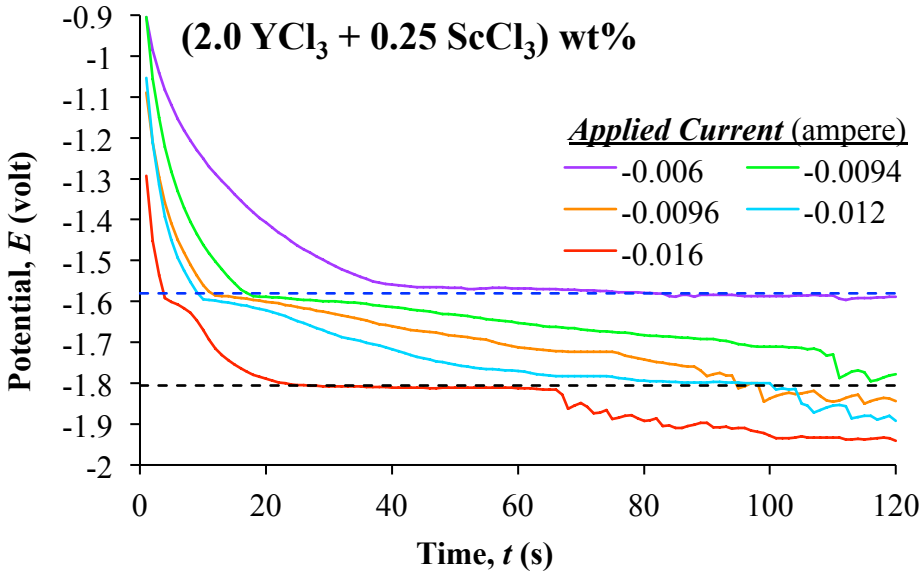

Figure 9: Chronopotentiometry plots of (2.0 YCl_3 + 0.25 $ScCl_3$) wt% salt mixture.

Table 6: Estimated values of scandium and yttrium reduction potentials from CP plots measured of the (2.0 YCl_3 + 0.25 $ScCl_3$) wt% salt mixture.

	Reduction Potential (volt)	
Applied Current (ampere)	***Scandium***	***Yttrium***
-0.006	-1.553	-
-0.008	-1.571	-
-0.009	-1.584	-
-0.0092	-1.572	-
-0.0094	-1.580	-
-0.0096	-1.577	-
-0.01	-1.575	-
-0.012	-1.594	-
-0.014	-1.603	-1.809
-0.016	-1.592	-1.803
μ	-1.580	-1.806
σ	0.013	-
$\lvert c_v \rvert$	0.844	-

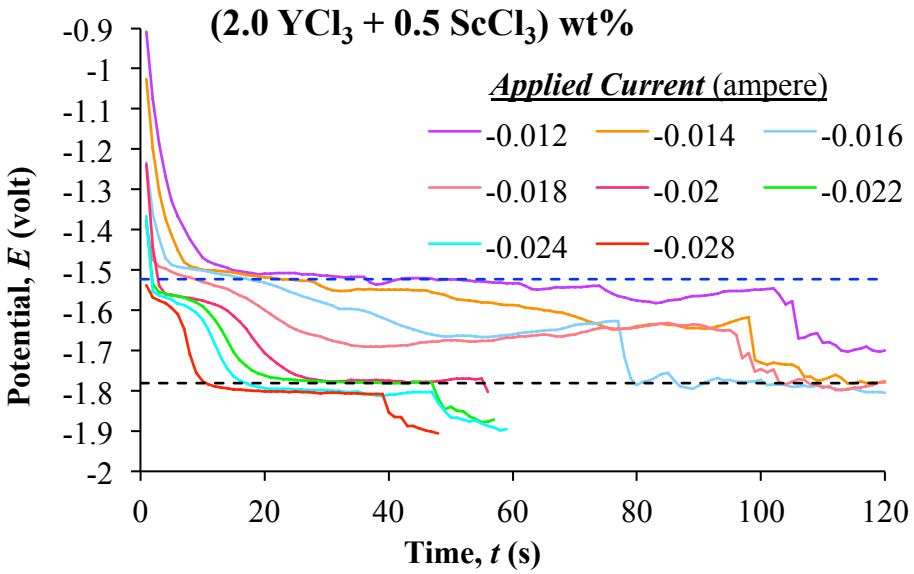

Figure 10: Chronopotentiometry plots of (2.0 YCl_3 + 0.5 $ScCl_3$) wt% salt mixture.

Table 7: Estimated values of scandium and yttrium reduction potentials from CP plots measured of the (2.0 YCl_3 + 0.50 $ScCl_3$) wt% salt mixture.

	Reduction Potential (volt)	
Applied Current (ampere)	***Scandium***	***Yttrium***
-0.028	-1.569	-1.793
-0.024	-1.554	-1.787
-0.022	-1.556	-1.768
-0.02	-1.560	-1.777
-0.018	-1.492	-
-0.016	-1.487	-
-0.014	-1.491	-
-0.012	-1.502	-
-0.008	-1.497	-
μ	-1.523	-1.781
σ	0.033	0.009
$\lvert c_v \rvert$	2.185	0.525

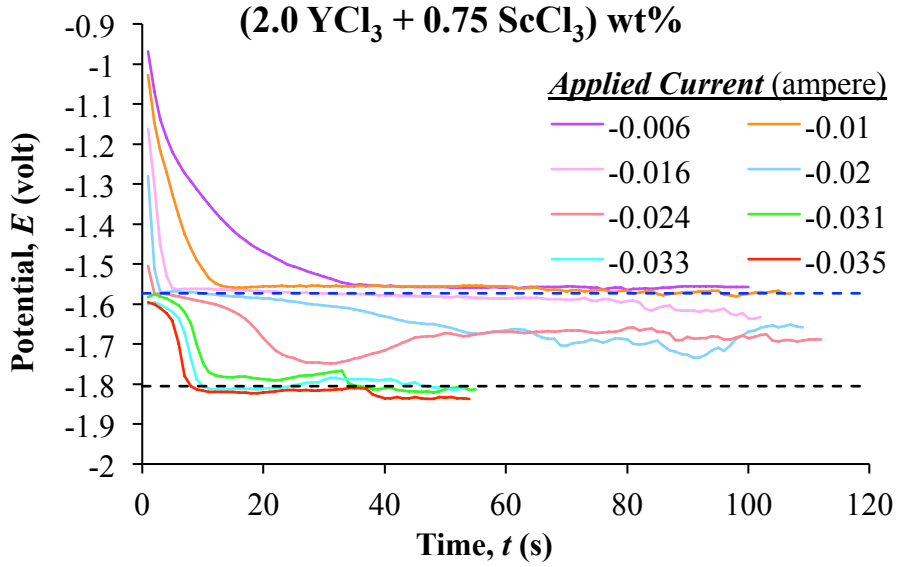

Figure 11: Chronopotentiometry plots of (2.0 YCl_3 + 0.75 $ScCl_3$) wt% salt mixture.

Table 8: Estimated values of scandium and yttrium reduction potentials from CP plots measured of the (2.0 YCl_3 + 0.75 $ScCl_3$) wt% salt mixture.

	Reduction Potential (volt)	
Applied Current (ampere)	***Scandium***	***Yttrium***
-0.006	-1.552	-
-0.01	-1.548	-
-0.016	-1.561	-
-0.02	-1.570	-
-0.024	-1.575	-
-0.031	-1.583	-1.784
-0.033	-1.600	-1.814
-0.035	-1.596	-1.820
μ	-1.573	-1.806
σ	0.018	-
$\lvert c_v \rvert$	1.142	-

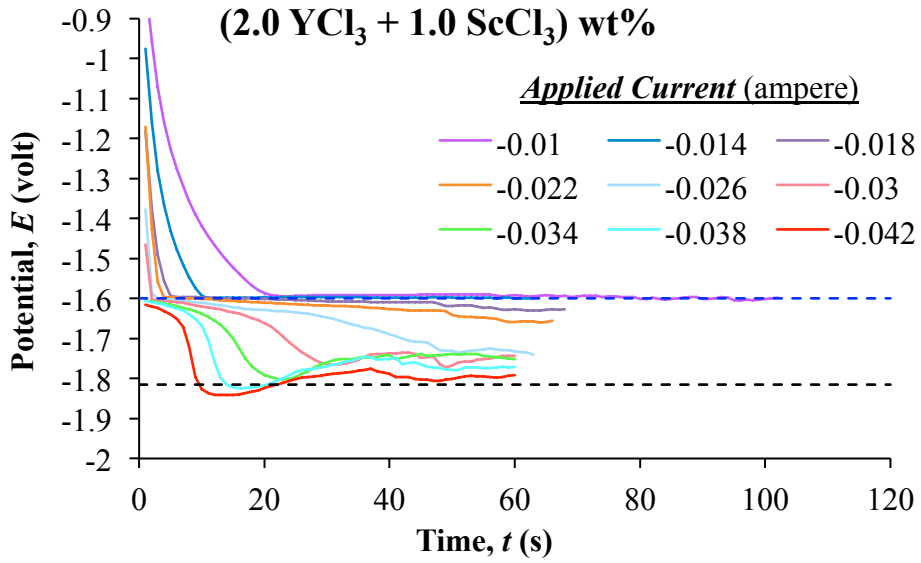

Figure 12: Chronopotentiometry plots of (2.0 YCl_3 + 1.0 $ScCl_3$) wt% salt mixture.

Table 9: Estimated values of scandium and yttrium reduction potentials from CP plots measured of the (2.0 YCl_3 + 1.0 $ScCl_3$) wt% salt mixture.

	Reduction Potential (volt)	
Applied Current (ampere)	***Scandium***	***Yttrium***
-0.01	-1.587	-
-0.014	-1.592	-
-0.018	-1.594	-
-0.022	-1.597	-
-0.026	-1.600	-
-0.03	-1.603	-
-0.034	-1.605	-1.798
-0.038	-1.605	-1.812
-0.042	-1.615	-1.836
μ	-1.600	-1.805
σ	0.008	0.007
$\lvert c_v \rvert$	0.491	0.371

In some cases the magnitude of the applied current was not great enough to cause a shift to the Y reduction potential. Thus, only the Sc reduction potential could be estimated. It can be seen as the magnitude of current is sufficiently increased, the curve tends toward more negative potentials and two plateaus become apparent. The plateaus correspond to Sc and Y reduction. Continued increase in the magnitude of current would affect the drop of potential to Li reduction.

There is discrepancy in estimation of reduction potential among the CV and CP measurement techniques. It seems using CP to estimate reduction potential would be more reliable, by looking for plateaus where the slope is close to zero. The values found by CP may also provide insight into a more accurate method to estimate reduction potential via CV. For example, finding the inflection point on the right-side of a reduction peak.

In general, as the concentration of $ScCl_3$ increases, the length of the Sc reduction plateau with respect to the *x*-axis increases and more current is required to drive the working electrode potential to the Y reduction potential. Based on the CP curves the Sc reduction potential appears to be in the range of - (1.55 to 1.60) V, whereas that of Y is - (1.80 to 1.85) V. The reduction potentials estimated from the CP data is closer to the reduction peak potentials in the CV curves whereas the onset potentials are more positive.

A feature common to the CP data at all concentrations of $ScCl_3$ is that at relatively small applied current, the working electrode potential is fairly stable after reaching the Sc reduction potential. Examples are – (0.006 and 0.01) A with (0.25 and 0.75) wt% $ScCl_3$, respectively. This seems to indicate that a reasonably pure Sc deposit is achievable, but would be a time extensive process, meaning low recovery rate.

Another feature amongst the CP plots at all concentrations of $ScCl_3$ is the deviation of the measured potential from the estimated reduction of Sc and Y at the intermediate applied currents. At these applied currents, the change of potential is relatively slow and not smooth with time. The observed drift in potential is likely due to the change in surface area of the electrode under deposition, and the resulting effect on diffusion layer surrounding the electrode.

At the relatively large applied currents, the transition from the Sc reduction to Y reduction is relatively fast and potential changes smoothly. Interestingly, in some cases, the potential reaches a minimum value and subsequently increases with time. In other cases the potential tends to drift toward the negative, which would be toward lithium as the next reducing species. Here again, the observed drifting of potential could be due to the change in electrode surface as Sc and Y are deposited. The observed drift in potential at intermediate and large applied currents seems to be the indication of the difficulty in controlling deposition of elements on the electrode.

4. CONCLUSIONS AND RECOMMENDATIONS

A careful examination of published data shows $ScCl_3$ and YCl_3 are adequate surrogates for UCl_3 and $PuCl_3$, respectively, in terms of difference in reduction potential. Regarding CV data in general, centering the *x*-axis to the Li or Y reduction potential and non-dimensionalizing the *y*-axis data with the Y peak current value provided a convenient and simple method to compare data generated with differing reference electrodes, working electrode surface areas, and scan rates. Scaling CV data according to Y reduction potential and peak current in this work may offer some encouragement to employ an internal standard in electrochemical measurements.

Cyclic voltammetry and chronopotentiometry data were successfully obtained of YCl_3 at fixed concentration and $ScCl_3$ at varying concentration in LiCl-KCl eutectic at 500 °C. Cyclic voltammetry plots were useful to identify the potential at which Sc and Y would reduce and confirm the potential difference between the two were close to that of U and Pu. The CV data also provided information as to what would be expected in chronopotentiometry data. The relationship of reduction potentials measured in this work match reasonably well with that estimated of literature values.

Chronopotentiometry data indicates as the concentration of $ScCl_3$ in the salt increases, higher applied currents are required to affect deposition of Y. At relatively low applied current stable Sc reduction potential can be achieved without depositing Y. As a consequence of small applied current, recovery rate is low. At intermediate applied currents, Sc deposition occurs, but the potential drifts between the Sc and Y reduction and somewhat erratically. When relatively large currents are applied, the measured potential was shown to drift in the positive or negative direction. While recovery rate at intermediate and large applied current is faster, it appears control of the deposit composition is more difficult. It is thought the drifting of measured potential results from a changing surface area under deposition and diffusion layer surround the electrode.

It is recommended that future work be a continuation of testing of the YCl_3-$ScCl_3$-ClLiK salt system with emphasis on long-duration CP measurements over a wider range of applied currents. Because CP

measurements imply deposition of Sc and Y on the electrode, it is recommended that working electrodes be removed from the molten salt at the conclusion of CP measurements such that deposits can be analyzed by such techniques as inductively coupled plasma-mass spectroscopy (ICP-MS). It is also recommended that effort be devoted to develop a more effective method of deposit sample preparation. The intent is to reduce deposit loss and avoid its involvement in chemical recations during sample preparation that affect accurate data collection.

5. REFERENCES

1. **Bermejo**, M.R.; Gomez, J.; Medina, J.; Martinez, A.M.; and Castrillejo, Y. "The Electrochemistry of Gadolinium in the Eutectic LiCl-KCl on W and Al Electrodes." *Journal of Applied Electroanalytical Chemistry*. 588, 253-266, **2006**. http://www.sciencedirect.com/science/article/pii/S0022072806000350
2. **Castrillejo**, Y.; Bermejo, M.R.; Martinez, A.M.; and Diaz Arocas, P. "Electrochemical Behavior of Lanthanum and Yttrium Ions in Two Molten Chlorides with Different Oxoacidic Properties: The Eutectic LiCL-KCl and the Equimolar Mixture $CaCl_2$-NaCl." *Journal of Mining and Metallurgy*. 39, (1-2) B, 109-135, **2003**. http://www.doiserbia.nb.rs/img/doi/1450-5339/2003/1450-53390302109C.pdf
3. **Castrillejo**, Y.; Hernandez, P.; Rodriguez, J.A.; Vega, M.; and Barrado, E. "Electrochemistry of Scandium in the Eutectic LiCl-KCl." *Electrochimica Acta*. 71, 166-172, **2012**. http://www.sciencedirect.com/science/article/pii/S0013468612004768
4. **Cruze**, T. A.; Blaskovitz, R.J.; Willit, J.L.; and Williamson, M.A.; "Solid Cathode Co-Deposition Prototype Development"; Department of Energy, Fuel Cycle Research & Development, FCRD-MRWFD- 2015-000006 (OUO and AT), August 30, **2015**.
5. **Fredrickson**, G. L.; "Recommend U/TRU Recovery Technology for Production Treatment of EBR-II Blanket Fuel (Revision 1)"; Department of Energy, Advanced Fuel Cycle Initiative, AFCI-SEPA-PMO-MI-DV-2009-000231 (OUO and AT), October 15, **2009**.
6. **Gese**, N.J.; Yoo, T-S; Serrano, B.E.; Fredrickson, G.L.; and Li, S. X. "FY-15 U/TRU Codeposition Technical Report." Department of Energy, Fuel Cycle Research & Development, FCRD-MRWFD-2015-000261 (OUO and AT), September 30, **2015**.
7. **Martinez**, A.M.; Borresen, B.; Haarberg, G.M.; Castrillejo, Y.; and Tunold, R. "Electrodeposition of Magnesium from the Eutectic LiCl-KCl Melt." *Journal of Applied Electrochemistry*. 34, 1271-1278, **2004**. http://link.springer.com/article/10.1007/s10800-004-1761-6
8. **Shaltry**, M.R.; Hoover, R.O.; Yoo, T.-S.; Gese, N.J.; Serrano, B.E.; Fredrickson, G.L. and Li, S.X. "FY-16 U/TRU Codeposition Technical Report." Department of Energy, Fuel Cycle Research and Development, FCRD-MRWFD-2016-000050 (OUO), September 15, **2016**.
9. **Shirai**, O.; Yamana, H.; and Arai, Y. "Electrochemical Behavior of Actinides and Actinide Nitrides in LiCl-KCl Eutectic Melts." *Journal of Alloys and Compounds*. 408-412, 1267-1273, **2006**. http://www.sciencedirect.com/science/article/pii/S092583880500681X
10. **Tylka**, M. M.; Willit, J.L.; and Williamson, M. A.; "FY2011 U/TRU Codeposition and Process Monitoring Studies"; Department of Energy, Fuel Cycle Research & Development, FCRD-SWF-2011-000420 (OUO and AT), September 16, **2011**.
11. **Willit**, J.L. and Williamson, M. A.; "Behavior of Solid Cathode Electrochemistry Under Off-Normal Conditions"; Department of Energy, Fuel Cycle Research & Development, FCRD-SWF-2012-000099 (OUO and AT), April 6, **2012**.

12. **Vaden**, D.; Li, S.X.; Westphal, B.R.; Davies, K.B.; Johnson, and T.A.; Pace, D.M.; "Engineering-Scale Liquid Cadmium Cathode Experiments," *Nuclear Technology*, v. 162, pp. 124-128, **2008.**